RSC Advances

PAPER

View Article Online
View Journal | View Issue

Cite this: *RSC Adv.*, 2021, **11**, 33883

Enhancement of antibacterial function by incorporation of silver-doped ZnO nanocrystals onto a laser-induced graphene surface

Liyong Wang,[a] Zhenghao Wang,[a] Zhiwen Wang,[a] Chunyang Zhang,[b] Yongling Wu*[a] and Hongyu Zheng *[a]

Bacterial biofilms formed on touchable surfaces such as displays of electronic devices not only reduce the product service life, but also cause human health issues. There is an urgent need to research the biofilm formation mechanism and methodologies to prevent formation of biofilms on human touchable surfaces. It has been reported that laser-induced graphene (LIG) helps resist biofilm growth, which has been attributed to the atomic composition and sharp edges of graphene. However, LIG alone was not able to retard bacterial growth completely. It has been reported that LIG incorporated with silver (Ag) nanoparticles exhibited enhanced surface antibacterial activity. As a heavy metal, overdose of Ag is harmful to human health. Therefore, a new biocompatible antibacterial agent to replace or reduce the use of Ag is highly important. In this study, we investigate and compare the effect of LIG doped with two types of nanocrystals, *i.e.*, ZnO and silver (Ag)-doped ZnO, on antibacterial actions. A 355 nm ultraviolet (UV) laser was used to produce LIG on a watercolor paper substrate. Formation of few-layer graphene has been verified by Raman spectra. *Escherichia coli* (*E. coli*), a representative of Gram-negative bacteria and *Staphylococcus aureus* (*S. aureus*), a representative of Gram-positive bacteria were employed for the investigation of the bacteriostatic properties of the LIG paper substrate. Results show that with the incorporation of either the ZnO nanocrystals or the silver (Ag)-doped ZnO nanocrystals into LIG, the antibacterial effect became stronger. It is further shown that the Ag-doped ZnO nanocrystals have superior antibacterial performance to that of the ZnO nanocrystals. The Ag-doped ZnO nanocrystals are potentially an effective and biocompatible antibacterial agent and yet have a much reduced and acceptable level of Ag concentration.

Received 24th August 2021
Accepted 13th October 2021

DOI: 10.1039/d1ra06390a

rsc.li/rsc-advances

1. Introduction

Bacteria such as Lactobacillus and acetic acid bacteria are the most diverse organisms on earth and play a key role in affecting human health. Some bacteria are especially unfriendly to human beings, such as *Escherichia coli*, *Helicobacter pylori* and so on. According to statistics, 10 000 people die of bacterial biofilms on medical devices every year,[1] which makes people realize the harmfulness of biofilms and the importance of preventing them. In addition, the formation of biofilms reduces the service life of products and requires a significant amount of manual labor and material resources to maintain the proper function of the products.[2] Consequently, antibacterial biofilms are not only a social demand, but also a commercial requirement. It is, however, important to understand the biofilm formation mechanism and to research methodologies to prevent or retard biofilm growth. Development of an effective and biocompatible antibacterial surface or antibacterial biofilm has become critical.

Graphene is a monolayer two-dimensional (2D) carbon material, which is constituted by sp^2-hybridized carbon.[3,4] With superior thermal, electrical and optical properties, graphene has been widely applied in supercapacitors, sensors and solar cells.[5–8] Traditional methods of fabricating graphene, such as organic synthesis, oxidation–reduction and chemical vapor deposition, are not conducive to scalable production on account of their complex processes and low efficiency. Laser-induced graphene (LIG) has been extensively studied in recent years.[9–13] Lin[14] reported a novel approach to manufacturing graphene by using a commercial CO_2 laser. Jeong *et al.* fabricated graphene using a commercial UV laser.[15] Wang reported a comparative study of the LIG on polyimide by using a CO_2 laser and a 355 nm UV laser.[9] By controlling laser parameters and atmospheric conditions, morphology and hydrophobicity of the LIG can be altered.[16,17] Owing to exceptional physical and chemical properties, the LIG has broad applications in

[a]*Centre for Advanced Laser Manufacturing (CALM), School of Mechanical Engineering, Shandong University of Technology, Zibo 255000, Shandong, China. E-mail: zhenghongyu@sdut.edu.cn; ylwu06@sdut.edu.cn*

[b]*College of Life Sciences, Shandong University of Technology, Zibo 255000, Shandong, China*

mechanic sensors,[15,18,19] chemical sensors[20–22] and supercapacitors.[23–25] Subsequently, many polymers and natural materials have been converted to the LIG, including polydimethylsiloxane (PDMS),[18] bread, wood, *etc.*26 In recent years, antimicrobial nanocarbons has rapidly attracted the attention of many researchers because of its excellent antibacterial properties. In 2010, it was reported that both graphene oxide (GO) and reduced graphene oxide (rGO) showed strong antibacterial activity, which was attributed to the atomic composition and its sharp edges of graphene.[27,28] In addition, Zhang *et al.*[29] observed bacterial oxidative stress and cell wall puncturing. The surface functionalization and number of graphene layers were shown to affect its antibacterial behaviour.[30] It was reported that the LIG formed on polyimide (PI) were shown to strongly resist biofilm formation, because nanofibers on the LIG inhibited the attachment and proliferation of bacterial cells.[31] Although the LIG can resist biofilm growth, the material itself doesn't kill bacteria. Abhishek *et al.*[32] reported Ag-doped LIG exhibited potent surface antibacterial activity and antibiofilm action. Wu *et al.* synthesized ZnO nanocrystals by methanol solutions of zinc acetate dihydrate at a low temperature.[33–35] Petya *et al.*[36] reported the antibacterial effect of ZnO nanoparticles on cotton.

In this article, we aim to investigate and compare the effect of doping two types of nanocrystals, *i.e.*, ZnO and silver (Ag) doped ZnO, into the LIG formed on a water color paper substrate on antibacterial actions. The proposed ZnO nanocrystals doped the LIG has great potential to provide a biodegradable antibacterial solution.

2. Materials and methods

In this study, a 20 W ultraviolet (UV) laser with a wavelength of 355 nm was used to fabricate LIG on a water color paper. The focal spot size (assuming a Gaussian beam distribution) was calculated to be 30 μm. The specific laser parameters are given in Table 1. The UV laser power was set at 3 W and the paper substrate was positioned at a defocusing distance of 6 mm in order to reduce the power density on the substrate and to avoid damage to the substrate. The water color paper with thickness of 0.5 mm was purchased commercially. *Escherichia coli* (CMCC(B) 44103) and *Staphylococcus aureus* (CMCC(B) 26003) were bought from Xinyang Laiyao Biotechnology Co., Ltd.

Scanning electron microscopy (SEM) (Quanta 250 FEG, Thermo Fisher Scientific, 81 Wyman Street, Waltham, MA, USA) was employed to examine the micromorphology of the LIG. Raman spectroscopy (HR Evolution, spectrum range: 200–2100 nm, Horiba Scientific, France) was used to verify the formation of the LIG. The element composition can be measured by X-ray diffractometer (XRD) (D8 ADVANCE, BrukerAXS, Germany).

Table 1 Laser parameters used for treating the water color paper

	Scan speed	Repetition rates	Line spacing	Pulse width
UV laser	100 mm s^{-1}	200 kHz	10 μm	10 μs

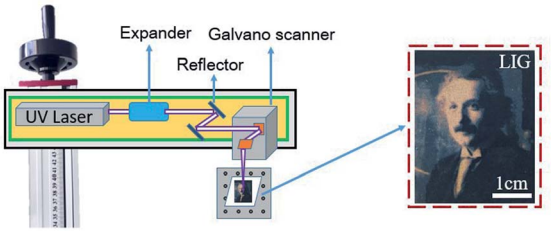

Fig. 1 Schematic diagrams of the laser operation process.

The schematic set-up for the laser operation is shown in Fig. 1. The UV laser beam is expanded before entering into a pair of the galvanometers, which control the movement of the laser beam. The focal radius, ω_f is determined by the following equation:

$$\omega_f = K_m \frac{1}{\pi} \frac{f_1 \lambda}{\omega_0} \quad (1)$$

where K_m is determined by the beam mode and is 1 for Gaussian beam, f_1 is the focal length, λ is the wavelength, and ω_0 is the entrance beam radius after the expander. The power density can be controlled by adjusting the focal spot radius for a given laser power.

In order to avoid the paper being ignited by the laser beam energy, the paper was soaked in flame retardant fluids ($FeCl_3$ and boric acid).[37] ZnO and Ag-doped ZnO nanocrystals were introduced to increase the antibacterial activity. The procedure of the sample preparation and the laser treating process are illustrated in Fig. 2.

The ZnO nanocrystals were obtained by dissolving the zinc acetate dihydrate in ethylene glycol in a molar ratio of 0.03 : 4, and were refluxed for 1.5 hours at 130 °C. The Ag-doped ZnO nanocrystals were prepared by dissolving the zinc acetate dehydrate and silver nitrate in ethylene glycol in a molar ratio of 0.03 : 0.006 : 4, and were refluxed for 1 hour at 130 °C. The ZnO and Ag-doped ZnO powder were washed by water and ethanol and dried in oven at 60 °C for 6 hours. The synthesis setup of Ag doped ZnO and the deposition process are illustrated in Fig. 3.

In the bacteriostatic experiments, the standard shake flask method, developed by the American Society for Testing and Materials for fabrics (ASTM-E2149-01), was used in

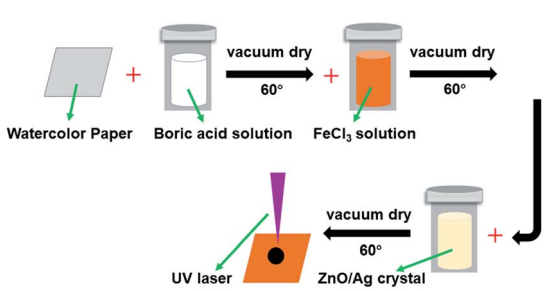

Fig. 2 Schematic process of flame retardant treatment.

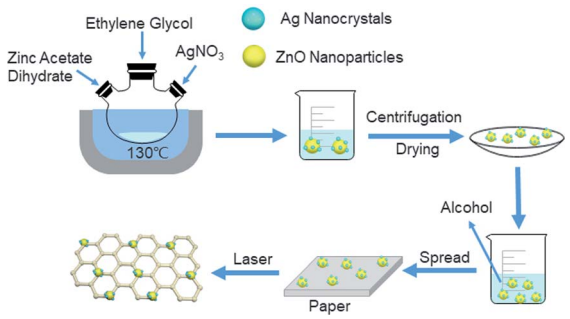

Fig. 3 Schematic diagram of the Ag doped ZnO synthesis setup and deposition process.

experiments. *E. coli* and *S. aureus* were incubated at 37 °C and 230 revolutions per minute (rpm) in sterile nutrient broth (NB). Sterile buffer (0.3 mM KH_2PO_4) was used to dilute the inoculated bacterial culture until the absorbance of the solution reached 0.28 ± 0.01 at 475 nm, which is equivalent to 1.5–3.0 × 10^8 colony forming units per milliliter (CFU mL^{-1}). Then this bacterial solution was diluted 1000 times (1.5–3.0 × 10^5 CFU mL^{-1}). Subsequently, 35 mg of the samples was shaken in 5 mL bacterial suspension (1.5–3.0 × 10^5 CFU mL^{-1}) at 37 °C and 230 rpm for 1 hour. 35 mg LIG with Ag doped ZnO contains about 1.75 mg of ZnO and 0.35 mg of Ag. When added to 5 mL of bacterial solution, it is equivalent to 350 μg mL^{-1} of ZnO and 70 μg mL^{-1} of Ag. The suspensions were diluted and coated on plate counting agar, and then cultured for 24 hours at 37 °C to count the number of bacterial colonies.

Antibacterial ability refers to percentage of bacteria reduction, which is the ratio between the average number of surviving bacteria before (B) and after (A) contact with samples[36] using the following formula:

$$\text{Bacteria reduction } (\%) = \frac{B - A}{B} \times 100 \quad (2)$$

3. Results and discussion

Using the processing parameters provided in Table 1, and laser power density of 6.6 × 10^3 W cm^{-2} the 355 nm UV laser was employed to investigate formation of graphene on the water color paper substrate. From the optical appearance, the laser-treated surface became darkened mainly due to the photothermal effect of the 355 nm beam interaction with the paper substrate, which carbonizes the paper. Using this method, the Einstein's portrait was printed on the paper substrate with varying darkness levels. The laser-treated samples were then

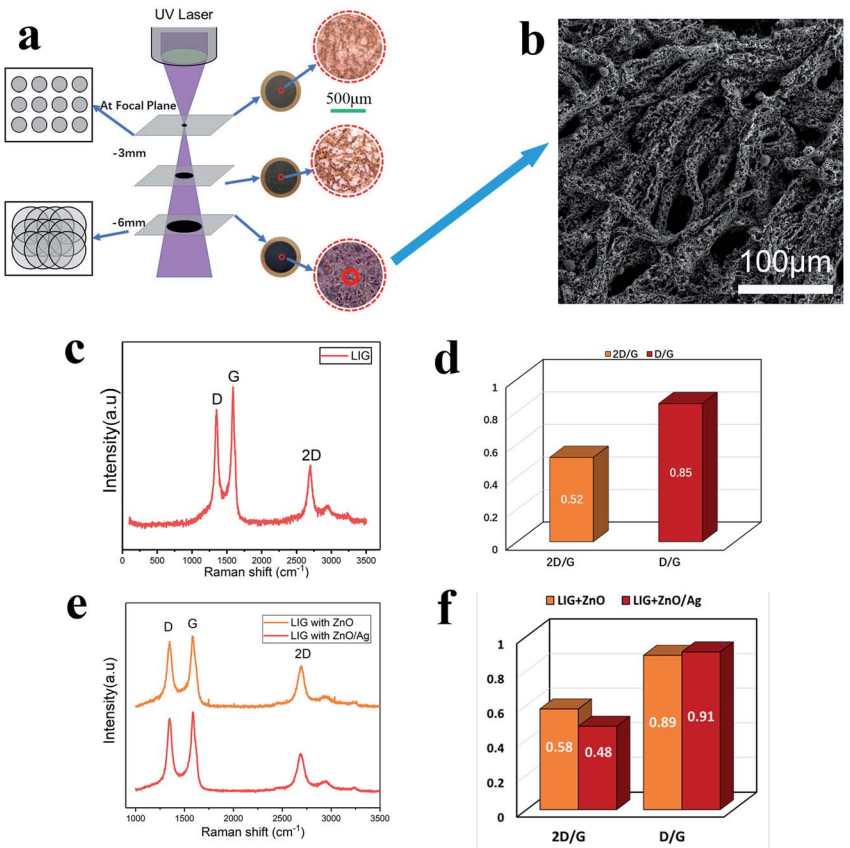

Fig. 4 (a) Schematic setup showing laser processing at different focal positions. (b) SEM images of LIG. (c) Raman spectrum of LIG and (d) the corresponding 2D/G and D/G peak ratios. (e) Raman spectra of LIG with ZnO nanocrystals and Ag doped ZnO nanocrystals respectively and (f) the corresponding 2D/G and D/G peak ratios.

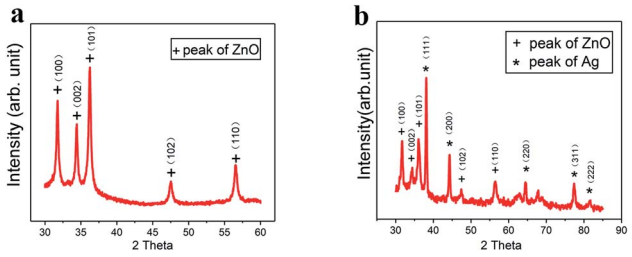

Fig. 5 XRD spectra of (a) ZnO powders and (b) Ag doped ZnO powders.

investigated for surface morphology analysis and chemical composition analysis in order to confirm the formation of the LIG on the substrate surface.

3.1 Morphological characterization and chemical composition analysis

As the UV laser beam focal spot size is only 30 μm, the efficiency of treating a large surface is low. Furthermore, the high-power density and high single-photon energy at focus was found to cause material ablation and thermal damage to the paper substrate. Consequently, the laser beam was defocused at a distance of 6 mm below the focal position (Fig. 4a), which led to the increased beam diameter of 210 μm and the reduced power density of 4.2×10^5 W cm^{-2} The enlarged beam diameter significantly reduced the total scanning time over a fixed scanning area. At the focal plane, a small area of material was ablated with barely noticeable carbonization. When the defocusing distance was increased to 3 mm, the laser irradiated area increased with a slightly more carbonization. With further increase in the defocusing distance to 6 mm, the laser-irradiated area became fully carbonized. Fig. 4b shows the SEM image of the surface micro-structures produced at the defocusing distance of 6 mm. There are many pores in the fibers of the paper substrate, which help to contain the ZnO nanocrystals and the Ag-doped ZnO nanocrystals. Raman spectral analysis was performed, which shows three distinguished peaks (Fig. 4c). These peaks are typical characteristics of laser-induced-graphene (LIG). The D peak at 1350 cm^{-1} is used to characterize defects in the LIG. The number of the LIG layers can be indicated by the G peak at 1580 cm^{-1} and the 2D peak at 2700 cm^{-1}. The appearance of sharp 2D peak proves the formation of graphene. Fig. 4d shows the ratio of D to G and 2D to G. The ratio D/G is 0.85, which implied some defects in the LIG.[12] The ratio 2D/G is 0.52, which indicates that a few-layered graphene has been formed. The result is in agreement with the previous studies.[28] After incorporating ZnO nanocrystals and Ag-doped ZnO nanocrystals onto the paper substrate, the Raman spectra of the laser-processed surfaces are shown in Fig. 4e, and the corresponding peak ratios are shown in Fig. 4f. Compared to the pristine LIG, the D to G ratios changed slightly, but did not influence the multi-layer character of graphene, while the 2D to G ratios increased indicating the existence of nanocrystals on the graphene surface as "defects".

To characterize the self-formulated ZnO nanocrystals, X-ray diffraction (XRD) was performed as shown in Fig. 5a. It indicates that there are five distinctive peaks in the 2θ 30–60° range, which confirms the presence of almost pure ZnO. ZnO is a semiconductor material with excellent biocompatibility, and has antibacterial and protective effects. Fig. 5b shows the XRD of the Ag-doped ZnO. Five characteristic peaks of Ag and five characteristic peaks of the ZnO in the 2θ 30–90° range are clearly shown indicating the co-existence of both Ag and ZnO in the powder.

With the UV laser irradiation, the water color paper substrate was photo-thermalized into the LIG. The laser irradiated area was decomposed by releasing gaseous products such as oxygen due to the photo-thermal effect. Meanwhile, the carbon atoms form the porous LIG. In the process of carbonization, the ZnO nanocrystals were attached to the surface and pores of the LIG

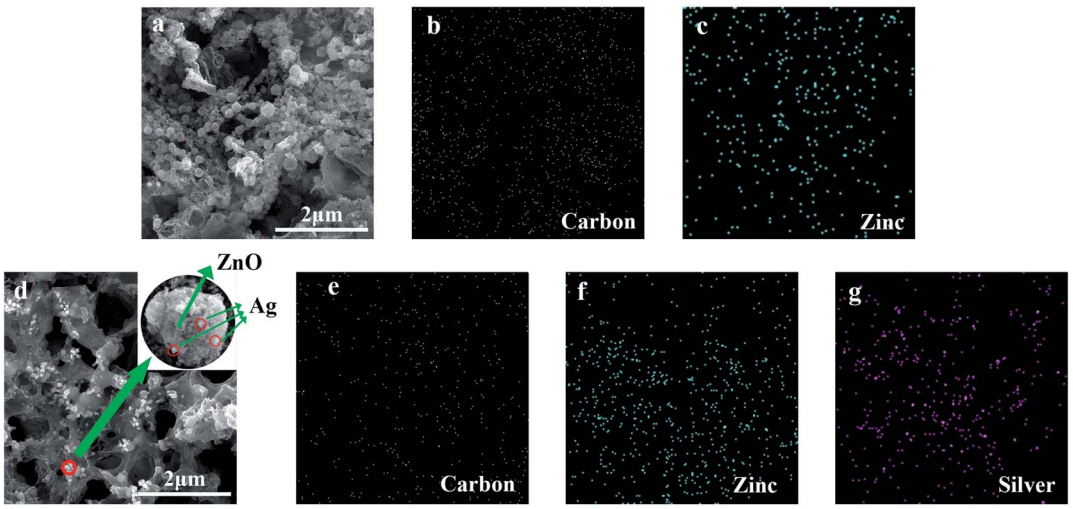

Fig. 6 (a) SEM image of LIG with ZnO. The EDS mapping of (b) carbon, (c) zinc on LIG with ZnO. (d) SEM image of LIG with Ag doped ZnO. The EDS mapping of (e) carbon, (f) zinc and (g) silver of LIG with Ag doped ZnO.

(Fig. 6a). It can be seen from the energy dispersive spectrometer (EDS) mapping that the carbon (Fig. 6b) and zinc (Fig. 6c) were evenly distributed on the surface of LIG. Similarly, after the laser irradiation, the Ag-doped ZnO nanocrystals were attached to the surface and pores of the LIG. Ag is physically adsorbed on the surface of ZnO (Fig. 6d). The carbon (Fig. 6e), zinc (Fig. 6f) and silver (Fig. 6g) were also uniformly distributed on the surface of LIG. The nanocrystal size was measured about 55 nm, some of which were amalgamated into sub-micron crystals.

3.2 Bacteriostatic effect

In our study, *E. coli* and *S. aureus* were employed to evaluate the antibacterial efficiency of the LIG incorporated with the ZnO and the Ag-doped ZnO nanocrystals.

By using the standard shake flask method, it can be observed through experiments that there are a large amount of *E. coli* (Fig. 7a) and *S. aureus* (Fig. 7b) colonies in the culture dish. When the paper substrate surface was converted into the LIG without the nanocrystals, the LIG incorporated with the ZnO nanocrystals, and the LIG incorporated with the Ag-doped ZnO nanocrystals, the number of bacterial colonies decreased accordingly. The LIG have a small inhibitory effect on both *E. coli* and *S. aureus*, which is caused by the addition of chemical flame retardant. After incorporating the ZnO nanocrystals, bacteriostasis has been greatly improved. When compared to the ZnO nanocrystals, the Ag-doped ZnO nanocrystals has a stronger inhibitory effect. Overdose of Ag is harmful to human health, ZnO has excellent biocompatibility and bacteriostatic performance. Therefore, the Ag-doped ZnO nanocrystals is an attractive and outstanding method. Antibacterial ability refers to percentage of bacteria reduction. As is shown in Fig. 7c and d, the LIG have a small antibacterial effect, after incorporating ZnO nanocrystals, the LIG showed excellent antibacterial activity on both *E. coli* and *S. aureus*. After incorporating the Ag-doped ZnO nanocrystals, the LIG exhibited nearly 100% reduction of the viability on *E. coli* and 84% reduction of the viability on *S. aureus*. This antibacterial ability can protect the LIG devices from the harm of bacteria.

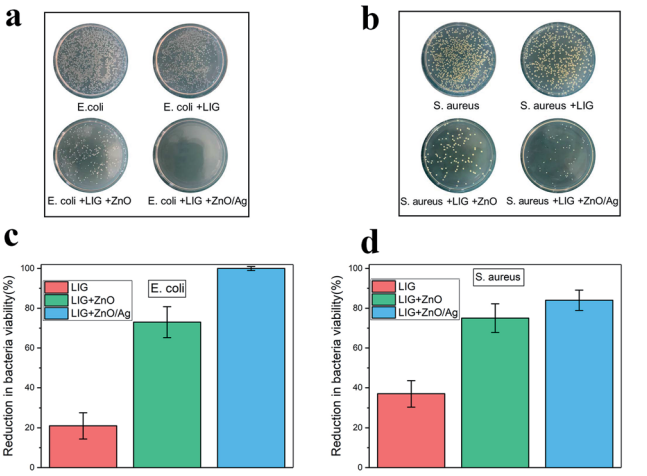

Fig. 7 Growth of (a) *E. coli* and (b) *S. aureus* colonies in different samples. Reduction in bacteria viability of (c) *E. coli* and (d) *S. aureus* in different samples.

ZnO nanocrystals and Ag nanoparticles are reported to have inhibitory effects on both Gram-positive and Gram-negative bacteria. There are differences in the cell compositions between Gram-positive bacteria and Gram-negative bacteria. Therefore, the antibacterial mechanism is also different. Gram-positive bacteria (*S. aureus*) has a thicker cell wall (20–80 nm).[38] While Gram-negative bacteria wall (*E. coli*) is composed of plasma membrane and outer membrane,[38] which is easy to be damaged by nanoparticles. The three antibacterial mechanisms of ZnO reported in the literature are: (1) ROS formation, (2) Zn^{2+} release, (3) electrostatic interactions.[39] In our study, no UV excitation was used in the experiment and incubation process. Therefore, Zn^{2+} release and electrostatic interactions are the main antibacterial mechanisms. The surface of bacteria is negatively charged, while ZnO is positively charged in solution.[40] Due to electrostatic interaction, ZnO nanocrystals are adsorbed on the surface of bacteria, pass through the cell wall, and destroy the cell membrane, resulting in disorder and leakage.[41] After Zn^{2+} entering the bacteria, they prevent the production of adenosine-triphosphate and interrupt the replication of DNA.[42] The minimum inhibitory concentration of ZnO was reported to be 3.1 and 1.5 mg mL^{-1} for *E. coli* and *S. aureus*, respectively.[39] The abundant negative charge on Gram-negative bacteria (*E. coli*) is conducive to the interaction between Ag nanoparticles and bacterial cell membrane. Ag nanoparticles degrade lipopolysaccharide molecules and form pits to change the properties of membrane, penetrate bacteria and destroy DNA. Ag nanoparticles dissolves on the surface of bacteria to create Ag^{+}, which improves the killing efficiency of bacteria.[43] The cell wall of Gram-positive bacteria (*S. aureus*) is mainly composed of a thick peptidoglycan layer, which makes them difficult to penetrate. It is consistent with the fact that the effect of silver nanoparticles on the growth of Gram-negative bacteria is greater than that of Gram-positive bacteria. Mirzajani *et al.* reported the antibacterial activity of silver nanoparticles against *S. aureus*, in that silver nanoparticles can lead to the release of muramic acid into the culture medium, resulting in the distraction of cell wall.[44] The concentration of Ag nanoparticles for thorough sterilization was reported to be 25 and 100 μg mL^{-1} for *E. coli*[45] and *S. aureus*,[46] respectively. In our study, 350 μg mL^{-1} of ZnO and 70 μg mL^{-1} of Ag were used to study the bacteriostatic effect. The antibacterial activity of Ag-doped ZnO nanocrystals is significantly higher than that of single ZnO nanocrystals, which is due to the synergistic anti-bactericidal effect between Ag and ZnO.[43] The mechanism of Ag doped ZnO nanocrystals antibacterial activity is illustrated in Fig. 8.

In the SEM observation (Fig. 6d), Ag is physically adsorbed on the surface of ZnO nanocrystals as shown in Fig. 6d. Comparing the XRD spectra of Fig. 5a and b, the relative higher (100) peak in Ag-doped ZnO crystal indicates some constraint of crystal growth by Ag attachment, implies the existence of chemical bond between Ag and ZnO (100) facets. This chemical bond could be a weak adsorption, which can be released when being added into bacteria cells, leading to good bacteriostatic effect. Therefore, the higher antibacterial activity of Ag-doped

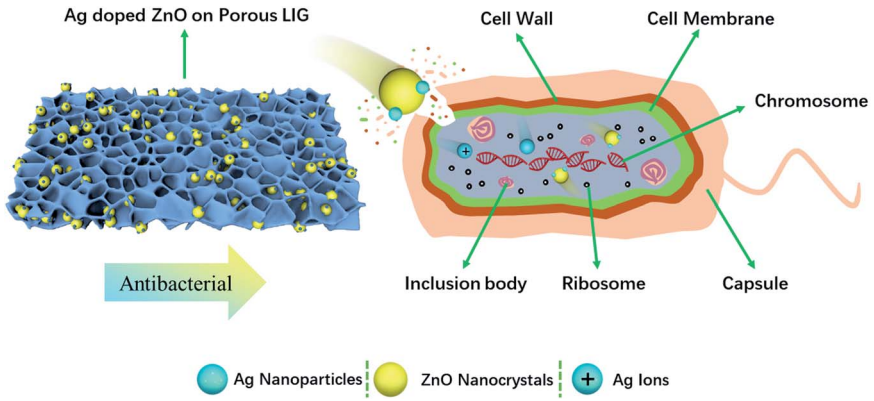

Fig. 8 Schematic diagram of antibacterial mechanism of Ag doped ZnO nanocrystals.

ZnO nanocrystals than single ZnO nanocrystal is the synergistic anti-bactericidal effect combining Ag and ZnO.

4. Conclusion

We provide a new approach for enhancing antibacterial function by incorporating self-formulated ZnO and Ag-doped ZnO nanocrystals into a LIG formed on a watercolour paper substrate by a UV laser. A 355 nm UV laser was used to convert the paper into LIG as evidenced by the Raman spectra. The EDS mapping shows that the ZnO and the Ag-doped ZnO nanocrystals were evenly distributed on the LIG surface. Two typical bacteria, *E. coli* and *S. aureus*, were utilized to measure the bacteriostatic properties of the laser-treated substrate surfaces. The standard shake flask method shows that the LIG with the Ag-doped ZnO nanocrystals exhibited nearly 100% reduction of the viability of *E. coli* and 84% reduction of the viability of *S. aureus*. The antibacterial mechanisms of Ag-doped ZnO are explained for Gram-negative and Gram-positive bacteria respectively. The self-formulated Ag-doped ZnO nanocrystals contain significantly lower level of Ag and are potentially an effective and biocompatible antibacterial agent.

Conflicts of interest

There are no conflicts of interest to declare.

Acknowledgements

This work was supported by the Taishan Scholar Project of Shandong Province [grant number ts20190401]; Shandong Natural Science Foundation [ZR2020ME164, ZR2020ME047].

References

1 A. K. Epstein, T. S. Wong, R. A. Belisle and E. M. Boggs, *Proc. Natl. Acad. Sci. U. S. A.*, 2012, **109**, 13182–13187.
2 J. Mansouri, S. Harrisson and V. Chen, *J. Mater. Chem. C*, 2010, **20**, 4567–4586.
3 A. K. Geim and K. S. Novoselov, *Nat. Mater.*, 2007, **6**, 183–191.
4 A. K. Geim, *Science*, 2009, **324**, 1530–1534.
5 F. Chong, M. Li, H. Li, C. Li, C. Qu and H. Yang, *Mater. Sci. Eng. C*, 2017, **72**, 425–432.
6 G. Liu, W. Jin and N. Xu, *Chem. Soc. Rev.*, 2015, **44**, 5016–5030.
7 X. Wang, L. Zhi and K. Müllen, *Nano Lett.*, 2008, **8**, 323–327.
8 Y. Shao, J. Wang, H. Wu, J. Liu, I. Aksay and Y. Lin, *Electroanalysis*, 2010, **22**, 1027–1036.
9 L. Wang, Z. Wang, A. N. Bakhtiyari and H. Zheng, *Micromachines*, 2020, **11**, 1094.
10 Z. Wang, W. Liu, W. Yuan, J. Cong, P. Chander, Y. Wu and H. Zheng, *J. Mater. Res. Technol.*, 2021, **12**, 2407–2413.
11 W. Yang, W. Zhao, Q. Li, H. Li, Y. Wang, Y. Li and G. Wang, *ACS Appl. Mater. Interfaces*, 2019, **12**, 3928–3935.
12 Z. You, Q. Qiu, H. Chen, Y. Feng, X. Wang, X. Wang and Y. Ying, *Biosens. Bioelectron.*, 2019, **150**, 111896.
13 G. Karimi, I. Lau, M. Fowler and M. Pope, *Int. J. Energy Res.*, 2021, **45**, 13712–13725.
14 J. Lin, Z. Peng, Y. Liu, F. Ruiz-Zepeda, R. Ye, E. L. Samuel, M. J. Yacaman, B. I. Yakobson and J. M. Tour, *Nat. Commun.*, 2014, **5**, 5714.
15 S. Y. Jeong, Y. W. Ma, J. U. Lee, G. J. Je and B. S. Shin, *Sensors*, 2019, **19**, 4867.
16 M. Abdulhafez, G. N. Tomaraei and M. Bedewy, *ACS Appl. Nano Mater.*, 2021, **4**, 2973–2986.
17 R. Ye, D. K. James and J. M. Tour, *Acc. Chem. Res.*, 2018, **51**, 1609–1620.
18 Y. Zhu, H. Cai, H. Ding, N. Pan and X. Wang, *ACS Appl. Mater. Interfaces*, 2019, **11**, 6195–6200.
19 M. G. Stanford, K. Yang, Y. Chyan, C. Kittrell and J. M. Tour, *ACS Nano*, 2019, **13**, 3474–3482.
20 A. R. Cardoso, A. C. Marques, L. Santos, A. F. Carvalho and E. Fortunato, *Biosens. Bioelectron.*, 2019, **124–125**, 167–175.
21 Y. Yang, Y. Song, X. Bo, J. Min, O. S. Pak, L. Zhu, M. Wang, J. Tu, A. Kogan and H. Zhang, *Nat. Biotechnol.*, 2020, **38**, 217–224.
22 Y. Zhang, H. Zhu, P. Sun, C. Sun and K. Qin, *Electroanalysis*, 2019, **31**, 1334–1341.
23 L. Li, J. Zhang, Z. Peng, Y. Li, C. Gao, Y. Ji, R. Ye, N. D. Kim, Q. Zhong, Y. Yang, H. fei, G. Ruan and J. M. Tour, *Adv. Mater.*, 2016, **28**, 838–845.

24 X. Li, W. Cai, K. S. Teh, M. Qi and L. Lin, *ACS Appl. Mater. Interfaces*, 2018, **10**, 26357–26364.
25 X. Shi, F. Zhou, J. Peng, R. Wu, Z. Wu and X. Bao, *Adv. Funct. Mater.*, 2019, **29**, 1902860.
26 Y. Chyan, R. Ye, Y. Li, S. P. Singh, C. J. Arnusch and J. M. Tour, *ACS Nano*, 2018, **12**, 2176–2183.
27 O. Akhavan and E. Ghaderi, *ACS Nano*, 2010, **4**, 5731–5736.
28 W. Hu, C. Peng, W. Luo, . Lv, X. Li and D. Li, *ACS Nano*, 2010, **4**, 4317–4323.
29 Y. Zhang, S. F. Ali, E. Dervishi, Y. Xu, Z. Li, D. Casciano and A. S. Biris, *ACS Nano*, 2010, **4**, 3181–3186.
30 X. Zou, L. Zhang, Z. Wang and Y. Luo, *J. Am. Chem. Soc.*, 2016, **138**, 2064–2077.
31 S. P. Singh, S. Ramanan, Y. Kaufman and C. J. Arnusch, *ACS Appl. Nano Mater.*, 2018, **1**, 1713–1720.
32 A. Gupta, L. Holoidovsky, C. Thamaraiselvan, A. K. Thakur, S. P. Singh and M. M. Meijler, *Chem. Commun.*, 2019, **55**, 6890–6893.
33 Y. Wu, C. S. Lim, S. Fu, A. I. Y. TOK, H. M. Lau, F. Y. C. Boey and X. Zeng, *Nanotechnology*, 2007, **18**, 15604.
34 Y. Wu, S. Fu, A. I. Y. Tok, X. Zeng, C. S. Lim, L. C. Kwek and F. Y. C. Boey, *Nanotechnology*, 2008, **19**, 345605.
35 Y. Wu, A. I. Y. Tok, F. Y. C. Boey, X. Zeng and X. Zhang, *Appl. Surf. Sci.*, 2007, **253**, 5473–5479.
36 P. Petkova, A. Francesko, I. Perelshtein, A. Gedanken and T. Tzanov, *Ultrason. Sonochem.*, 2016, **29**, 244–250.
37 Y. Chyan, J. Cohen, W. Wang, C. Zhang and J. M. Tour, *ACS Appl. Nano Mater.*, 2019, **2**, 3007–3011.
38 G. Fu, P. S. Vary and C.-T. Lin, *J. Phys. Chem. B*, 2005, **109**, 8889–8898.
39 A. Sirelkhatim, S. Mahmud, A. Seeni, N. H. M. Kaus, C. A. Ling, S. K. M. Bakhori, H. Hasan and D. Mohamad, *Nano-Micro Lett.*, 2015, **7**, 219–242.
40 L. Zhang, Y. Ding, M. Povey and D. York, *Prog. Nat. Sci.*, 2008, **18**, 939–944.
41 R. Wahab, Y. S. Kim, A. Mishra, S. I. Yun and H. S. Shin, *Nanoscale Res. Lett.*, 2010, **5**, 1675–1681.
42 C. N. Lok, C. M. Ho, R. Chen, Q. Y. He, W. Y. Yu, H. Sun, P. K. H. Tam, J. F. Chiu and C. M. Che, *J. Proteome Res.*, 2006, **5**, 916–924.
43 Y. Liu, C. Xu, Z. Zhu, J. Lu, A. G. Manohari and Z. Shi, *Mater. Res. Bull.*, 2017, **98**, 64–69.
44 F. Mirzajani, A. Ghassempour, A. Aliahmadi and M. Esmaeili, *Res. Microbiol.*, 2011, **162**, 542–549.
45 S. Shrivastava, T. Bera, A. Roy, G. Singh, P. Ramachandrarao and D. Dash, *Nanotechnology*, 2007, **18**, 225103.
46 O. Ibrahim, A. H. Saliem and S. I. Salih, *Al-Anbar J. Vet. Sci.*, 2016, **9**, 22–36.